inorganics

MDPI

Article

Eco-Friendly Fabrication of Zinc Oxide Nanoparticles Using *Gaultheria fragrantissima*: Phytochemical Analysis, Characterization, and Antimicrobial Potential

Bhoj Raj Poudel [1], Sujan Dhungana [1], Anita Dulal [1], Aayush Raj Poudel [2], Laxmi Tiwari [1], Devendra Khadka [3,4], Megh Raj Pokhrel [4], Milan Babu Poudel [5,*], Allison A. Kim [6] and Janaki Baral [1,*]

[1] Department of Chemistry, Tri Chandra Multiple Campus, Tribhuvan University, Kathmandu 44600, Nepal; bhoj.poudel@trc.tu.edu.np (B.R.P.); sujandhungana73@gmail.com (S.D.); aanitadulal@gmail.com (A.D.); tiwarilaxmi090@gmail.com (L.T.)
[2] Department of Chemistry, St. Xavier's College, Maitighar, Kathmandu 44600, Nepal
[3] Department of Chemistry, Tribhuvan Multiple Campus, Tribhuvan University, Tansen, Palpa 32500, Nepal; devendra.khadka@tmc.tu.edu.np
[4] Central Department of Chemistry, Tribhuvan University, Kirtipur, Kathmandu 44600, Nepal; meghrajpokhrel2000@ymail.com
[5] Department of Convergence Technology Engineering, Jeonbuk National University, Jeonju 54896, Republic of Korea
[6] Department of Healthcare Management, Woosong University, Daejeon 34606, Republic of Korea; allisonki@wsu.ac.kr
* Correspondence: poudelmeelan@gmail.com (M.B.P.); janaki.baral@trc.tu.edu.np (J.B.)

Abstract

This work explores zinc oxide nanoparticle (ZnO NP) synthesis utilizing leaf extract of the *Gaultheria fragrantissima* plant that are useful in medicine, environmental remediation, and cosmetics due to their antibacterial activity, photocatalytic efficiency, and UV-blocking characteristics. Traditional synthesis methods involve energy-intensive procedures and hazardous chemicals, posing environmental and human health risks. To overcome these limitations, this research focuses on utilizing *G. fragrantissima*, rich in bioactive compounds such as phenolics and flavonoids, with the methyl salicylate previously reported in the literature for this species, which helps reduce and stabilize NPs. ZnO NPs were characterized through X-ray diffraction (XRD), UV–visible spectroscopy, Fourier transform infrared (FTIR) spectroscopy, field emission scanning electron microscopy (FESEM), and energy-dispersive spectroscopy (EDS). The ZnO NPs were found to have a well-defined crystalline structure, with their average crystallite size measured at around 8.26 nm. ZnO NPs exhibited moderate antimicrobial activity against selected microbial strains. These findings underscore the potential of *G. fragrantissima*-mediated synthesis as an environmentally sustainable and efficient method for producing ZnO NPs with multifunctional applications. This study provides a greener alternative to conventional synthesis approaches, demonstrating a method that is both eco-friendly and capable of yielding NPss with desirable properties.

Keywords: *Gaultheria fragrantissima*; eco-friendly; ZnO NPs; bioactive; antimicrobial

check for updates

Academic Editor: David Morales-Morales

Received: 14 May 2025
Revised: 12 July 2025
Accepted: 17 July 2025
Published: 19 July 2025

Citation: Poudel, B.R.; Dhungana, S.; Dulal, A.; Poudel, A.R.; Tiwari, L.; Khadka, D.; Pokhrel, M.R.; Poudel, M.B.; Kim, A.A.; Baral, J. Eco-Friendly Fabrication of Zinc Oxide Nanoparticles Using *Gaultheria fragrantissima*: Phytochemical Analysis, Characterization, and Antimicrobial Potential. *Inorganics* **2025**, *13*, 247. https://doi.org/10.3390/inorganics13070247

Copyright: © 2025 by the authors. Licensee MDPI, Basel, Switzerland. This article is an open access article distributed under the terms and conditions of the Creative Commons Attribution (CC BY) license (https://creativecommons.org/licenses/by/4.0/).

1. Introduction

Recent progress in nanotechnology, especially in precisely synthesizing NPs with controlled size and shape, has opened new possibilities for creating innovative biocidal

agents. Numerous studies have demonstrated that NP-based formulations possess significant antimicrobial potential [1–3]. Inorganic NPs have been widely used as antimicrobial agents because they offer important advantages including less host toxicity, improved stability with longer durability, decreased microbial resistance, and good selectivity [4–6]. ZnO NPs offer additional advantages of enhanced selectivity, greater heat resistance, reduced cytotoxicity, and superior stability, making them more favorable than other inorganic NPs [7].

ZnO NPs exhibit remarkable properties, including chemical and physical stability, high catalytic activity, potent antibacterial effects, and strong absorption in the ultraviolet and infrared regions [8,9]. Due to these properties, ZnO NPs have potential applications in various fields, including solar cells, semiconductor devices, sensors, and transparent electrodes [10–12]. ZnO has attracted considerable attention owing to its unique optical, piezoelectric, and magnetic characteristics [13–15]. In addition, ZnO NPs hold promises for food and agriculture due to their antimicrobial effectiveness, offering a potential solution for developing safe, cost-effective alternatives to antibiotics against resistant pathogens in food processing [16–18]. Studies indicate ZnO NPs show selective toxicity toward cancer cells and demonstrate significant anticancer activity against cervical cancer (HeLa) cells and human brain tumors [19–21].

The unique properties of ZnO allow various methods to synthesize ZnO nanostructures by controlling the synthesis parameters. The selected method mostly depends on the desired application, as different methods produce different morphologies and sizes of ZnO particles [22]. Accordingly, the chemical and physical parameters such as pH, solvent type, precursors, and temperature were considered [23]. The most adopted fabrication methods include sol-gel, thermal evaporation of ZnO powders at 1400 °C, hydrothermal synthesis, simple thermal sublimation, self-combustion, polymerized complex method, physical–vapor, microwave irradiation, sol-gel, precipitation, and solution synthesis [24]. Green synthesis is widely employed for synthesizing ZnO NPs because it utilizes biological materials like plant extracts as stabilizing and reducing agents in an eco-friendly manner. However, conventional physical and chemical methods for ZnO NPs synthesis often involve toxic solvents, high temperatures, costly instrumentation, and environmental hazards, which restrict their scalability and sustainability [25,26]. Green synthesis, in contrast, offers a biocompatible and low-cost approach using plant-based reducing agents. In this context, the present study is novel as it utilizes *G. fragrantissima* aqueous leaf extract, which has not been previously reported for ZnO NPs synthesis. This plant is widely available in Nepal and contains a rich diversity of bioactive compounds, making it a promising candidate for sustainable nanomaterial development.

The study highlights a green synthesis of ZnO NPs using leaf extract of the plant *G. fragrantissima*, commonly known as "Dhasingre and Machino", which belongs to the family Ericaceae. The essential oil derived from *G. fragrantissima* is among the major exports from Nepal. Species of Gaultheria have been recognized for their medicinal properties, including the treatment of colds, rheumatoid arthritis, inflammatory diseases, pain, swelling, chronic tracheitis, and both acute and chronic prostatitis [27,28]. The analgesic and anti-inflammatory effects of Gaultheria are attributed to its methyl salicylate content [28,29]. Phytochemicals including alkaloids, flavonoids, quinone, sterols, tannins, terpenoids, reducing sugar, and saponin are abundant in *G. fragrantissima* leaf extract [27]. These bioactive compounds play the role of natural medium in reducing and stabilizing ZnO NPs, promoting eco-friendly synthesis. Compared to other plants, *G. fragrantissima* is abundantly available in the Himalayan region, especially in Nepal, and is economically viable due to its natural abundance. Its phytochemical richness makes it equally or more efficient in facilitating ZnO NPs synthesis.

This study examines ZnO NPs synthesized from *G. fragrantissima* using XRD, FTIR, FESEM, EDS, and UV–vis spectroscopy to analyze their size, morphology, and functional groups. It also evaluates the antimicrobial efficacy against strains of bacteria and fungi and the phytochemical screening in the plant extract. The study proposes tackling the challenges related to antimicrobial activity by proposing a sustainable alternative to conventional synthesis methods.

2. Results and Discussion

2.1. Phytochemical Screening

The plant leaf extract reveals the presence of several key compounds. The tests showed positive results for alkaloids, as indicated by Dragendroff's and Wagner's tests. Carbohydrates were also detected through positive results in both Benedict's and Molisch's tests. Reducing sugars was confirmed with Fehling's test. Glycosides were identified using the Killer–Killani test, and tannins were present as evidenced by Braymer's test. The presence of flavonoids was confirmed by the alkaline reagent test, and phenolics were detected using the ferric chloride test. Additionally, saponins were identified through the froth test. However, the ninhydrin test for proteins and amino acids yielded a negative result, suggesting that these compounds are not present in the extract. This comprehensive analysis highlights the diverse phytochemical profile of the methanol extract, which includes various bioactive compounds but lack detectable levels of proteins and amino acids. Table 1 displays the results of the phytochemical screening of *G. fragrantissima* leaf extract. Phytochemicals, especially phenolics and flavonoids, serve as natural reducing and stabilizing agents in the green synthesis of ZnO NPs [30]. By binding metal ions with their hydroxyl and carbonyl groups, phytochemicals like flavonoids and phenolics support the formation of NPs by acting as reducing and stabilizing agents. These compounds also exhibit considerable potential for antimicrobial applications. The inherent antimicrobial properties of flavonoids and tannins may enhance the bactericidal activity of ZnO NPs against pathogenic microorganisms [31]. Uncharacterized organic compounds in the extract may affect screening results, though this is unlikely and needs to be addressed in future targeted analyses.

Table 1. Phytochemical screening of the leaf extracts of *G. fragrantissima*.

S. N	Phytochemicals Compounds	Tests	Results
1.	Alkaloids	Dragendroff's test	+
		Wagner's test	+
2.	Carbohydrates	Benedict's test	+
		Molisch's test	+
3.	Reducing sugar	Fehling's test	+
4.	Glycosides	Killer–Killani test	+
5.	Tannins	Braymer's test	+
6.	Flavonoid	Alkaline reagent test	+
7.	Phenols	Ferric chloride test	+
8.	Saponin	Froth test	+
9.	Protein and amino acid	Ninhydrin test	−

2.2. Visual Observation

The synthesis mechanism involves three key stages. During the activation stage, zinc ions from the $ZnNO_3$ solution bind to reducing metabolites and stabilizing agents in the *G. fragrantissima* extract. These ions are subsequently reduced to zinc atoms, initiating nucleation. Next, in the growth stage, Ostwald ripening occurs, in which smaller NPs combine to form larger particles via heterogeneous nucleation and growth, accompanied

by further reduction of zinc ions. Finally, the NPs attain their final shape in the termination stage. After oxidation, stable and well-dispersed ZnO NPs are formed [32–34].

2.3. UV–Vis Analysis

The UV–visible data shows the absorbance of a sample within the range of 200 to 600 nm wavelength. The sharp peak observed at 358 nm in the spectrum of the bio-synthesized NPs, as shown in Figure 1a, serves as a characteristic feature that identifies ZnO NPs. A noticeable blueshift in the excitonic absorption peak was observed for the biogenic ZnO NPs (358 nm) compared to bulk ZnO (373 nm), indicating a size-dependent quantum confinement effect [35,36]. The spectrum revealed a single distinct peak, highlighting the exceptional purity of ZnO NPs produced via the synthesis using *G. fragrantissima*. The sharp, single absorbance peak at 358 nm, combined with calcination at 400 °C, ensures the removal of residual organics, confirming ZnO NPs as the primary absorbing species. This optical phenomenon suggests a quantum scale impact for these NPs. The optical band gap energies (Eg) of the samples were estimated using the Tauc equation (Equation (1)) [37].

$$Ah\nu = C\,(h\nu - E_g)^n \quad (1)$$

where h is Planck's constant (6.626×10^{-34} Js), c is the velocity of light ($3 \times 108\ ms^{-1}$), and λ is the absorption wavelength of synthesized biogenic ZnO NPs.

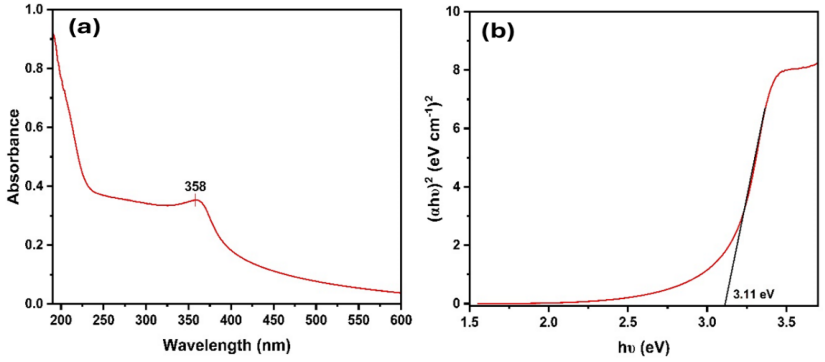


Figure 1. (**a**) UV absorbance spectrum and (**b**) Tauc plot with a band gap of ZnO NPs.

To gain insight into the optical bandgap of the synthesized ZnO NPs, a Tauc plot (Figure 1)) was generated using UV–vis absorption data, assuming a direct allowed electronic transition. The optical bandgap was determined by extrapolating the linear region of the $(\alpha h\nu)^2$ versus photon energy ($h\nu$) plot, resulting in a direct bandgap of approximately 3.11 eV. These values are less than the band gap of bulk ZnO (3.37 eV). Typically, as NPs get smaller, the absorption peak changes to a lower wavelength (blue shift), and the band gap widens. However, in this scenario, the ZnO NPs have a lower band gap than the bulk ZnO. This could be due to surface effects, such as overlapping energy levels near the surface, or the presence of defects that cause extra energy levels within the band gap [38]. Such properties make this material potentially useful for applications in UV detectors, optoelectronic devices, or as a UV-blocking layer in various technologies.

2.4. FTIR Analysis

The FTIR spectra of ZnO NPs (in red) and plant extract (in black) within the 400–4000 cm^{-1} range are shown in Figure 2a. The broad absorption peak in the 3100–3400 cm^{-1} range can be attributed to the absorption of hydroxyl groups (O–H) due to the presence of alcohols, phenols, or water in the plant extract [39]. The C-H stretching at 2922 cm^{-1} found in alkanes, while 1608 cm^{-1} suggests C=C stretching vibrations from aro-

matic compounds. Another peak at 1032 cm^{-1} corresponds to C-O, which could be linked to alcohols, ethers, or carbohydrate structures of phytochemicals in plant extract. ZnO NPs show a weak broad O-H stretching around 3293 cm^{-1} compared to the spectrum of plant extract. This suggests that the hydroxyl groups in the NPs are mostly due to the water molecules in NPs. Compared to the plant extract, there is a noticeable shift and reduction in intensity for peaks in the ZnO spectrum, indicating that extracting functional groups is crucial during the synthesis of ZnO NPs. The peak around 500 cm^{-1} is characteristic of Zn-O stretching, indicating the presence of ZnO. A similar result is seen in the published literature [40].

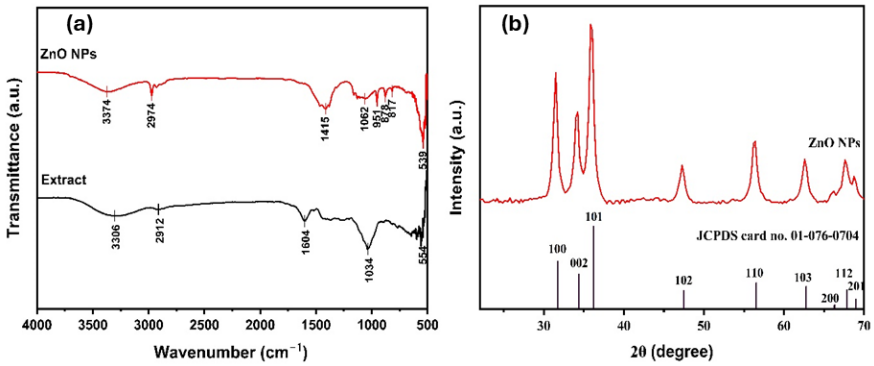


Figure 2. (**a**) FTIR spectroscopy of ZnO NPs (red) and plant extract (black); (**b**) XRD patterns of ZnO NPs synthesized using *G. fragrantissima* leaf extract.

2.5. XRD Analysis

X-ray diffraction was used to study the crystal structure and average crystallite size of the ZnO NPs. Figure 2b shows well-defined diffraction peaks within the 2θ range of 20° to 80°. The observed peaks correspond to specific Miller indices, namely (100), (002), (101), (102), (110), (103), (200), (112), and (201) with 2θ values recorded at 31.49°, 34.25°, 35.80°, 47.27°, 56.41°, 62.59°, 66.24°, 67.62°, and 68.76°, respectively. All these peaks reveal a crystalline nature of ZnO as characteristic of the hexagonal wurtzite structure (JCPDS Card No. 01-076-0704) [41]. The crystal structure of the sample was identified as hexagonal with the space group $P6_3mc$ (No. 186), which matches the typical wurtzite-type ZnO. The unit cell parameters were found to be a = b = 3.2530 Å and c = 5.2130 Å, with angles $\alpha = \beta = 90°$ and $\gamma = 120°$. The unit cell volume was calculated as 47.77 × 10^6 pm^3, and the theoretical density was 5.66 g/cm^3. The number of ZnO units per unit cell (Z) was 2. The corresponding interplanar spacings (*d*) are consistent with previously reported ZnO values [42]. For instance, in Table 2, the (100), (002), and (101) planes exhibit *d*-spacings of 2.82 Å, 2.61 Å, and 2.48 Å, respectively, confirming the wurtzite hexagonal structure. The strongest peak appeared at 35.80°, which corresponds to the (101) plane, suggesting that the crystals are mainly oriented along this direction.

The crystallite sizes of the synthesized ZnO NPs ranged from 3.91 to 11.60 nm, with an average size of about 8.26 nm using the Scherrer equation [43]. The observed crystallite size aligns well with values reported in similar studies, confirming the accuracy of both synthesis and analytical methods [44]. The smallest size, 3.91 nm, was seen at the diffraction angle 66.24°, likely due to peak broadening caused by lattice strain and very small particle size. This agrees with the findings of Yogamalar et al., who explained that peak broadening in XRD patterns is influenced by both crystallite size and microstrain, with strain effects becoming more noticeable at higher angles [45]. The sharp and narrow XRD peaks show that the particles are highly crystalline. This high crystallinity is likely due to the plant-based compounds in the *G. fragrantissima* extract, which helped in forming and stabilizing the NPs during green synthesis.

Table 2. The structural parameters of the ZnO NPs.

2θ (°)	Miller Indices (hkl)	FWHM (°)	d [Å]	Crystallite Size (nm)
31.49	(100)	0.69698	2.82	11.60
34.25	(002)	0.89336	2.61	9.04
35.80	(101)	0.74426	2.48	10.60
47.27	(102)	1.08634	1.91	7.45
56.41	(110)	0.94486	1.63	8.44
62.59	(103)	1.0367	1.48	7.62
66.24	(200)	2.01618	1.41	3.91
67.62	(112)	1.14293	1.38	7.06
68.76	(201)	0.9344	1.36	8.63

2.6. FESEM and EDS Analysis

The FESEM image offers insights into the structural and morphological characteristics of the sample analyzed. As shown in Figure 3, the image highlights an uneven, porous, rough, and aggregated structure. Porous and aggregated ZnO NPs were visible in the FESEM images; this morphology is frequently caused by natural polymeric capping agents found in plant extracts. This structure can enhance surface reactivity. The EDS analysis of the synthesized ZnO NPs provides valuable information about their elemental composition and distribution of Zn and O. As shown in Figure 3c, the EDS color mapping images depict the uniform distribution of the Zn and O throughout the materials. Furthermore, the EDS spectrum presented in Figure 3d, confirms the presence of zinc (Zn) and oxygen (O) with weight percentages of 59.78% and 40.22%, respectively. The peak near 1 keV corresponds to zinc (Zn Lα), and the peak around 0.5 keV corresponds to oxygen (O Kα). These findings validate the elemental makeup of the sample, with high Zn and O content confirming the successful synthesis of ZnO NPs. The absence of significant additional peaks suggests the sample purity, with no contamination from other elements.

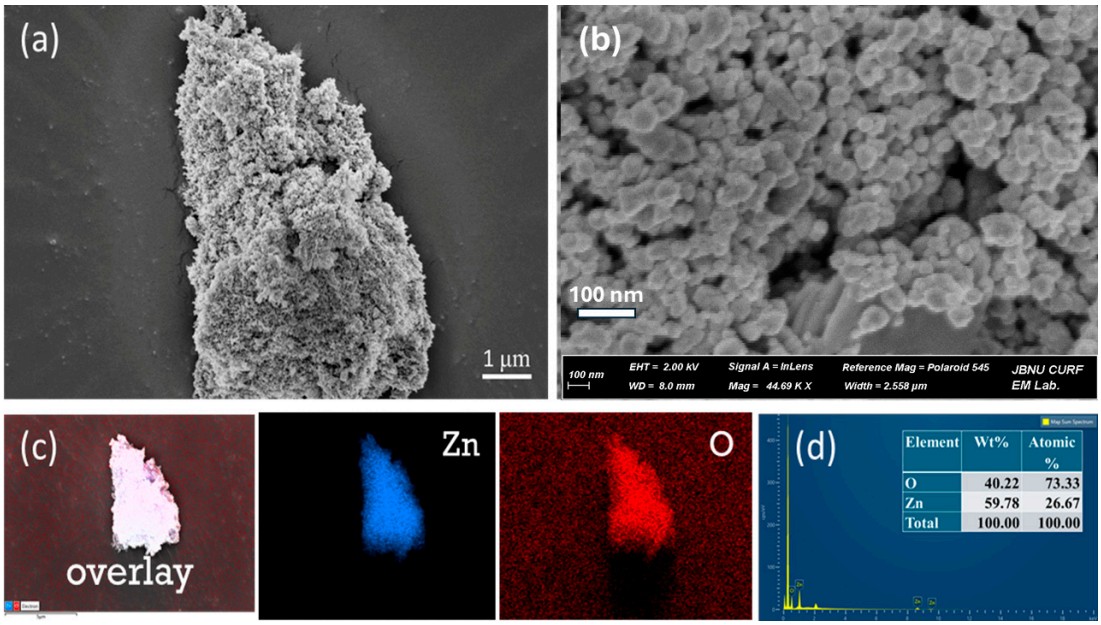


Figure 3. Morphological study of ZnO NPs (**a**) and (**b**) FESEM images of ZnO NPs at various magnifications, (**c**) EDX elemental mapping, and (**d**) EDX spectra.

2.7. Antimicrobial Activity

ZnO NPs tested for their antimicrobial properties against ATCC bacterial strains and a fungal strain through the agar well diffusion technique. The antibacterial capability of ZnO NPs was validated by a distinct inhibitory zone surrounding each well on the Petri plates, as seen in Figure 4. The findings are compiled in Table 3. All antimicrobial assays were performed in triplicates. Results are reported as mean ± standard deviation (n = 3). The ZnO NPs demonstrated a modest level of antibacterial activity. ZnO NPs showed an inhibition zone of 17 ± 0.2 mm against Gram-negative *E. coli* and 17 ± 0.3 mm Gram-positive *S. aureus*. For *C. albicans*, a fungal strain, the ZnO NPs resulted in an inhibition zone of 16 ± 0.4 mm. The plant extract had no inhibitory effect on the antimicrobial strains, with no inhibition zone. The use of distilled water, which might have limited the extraction of non-polar or less water-soluble bioactive compounds, is blamed for this lack of activity. The current study is limited by the absence of methanolic extracts, which are known to produce a wider variety of phytochemicals. The relative antimicrobial effectiveness of aqueous and methanolic plant extracts should be investigated in future studies.

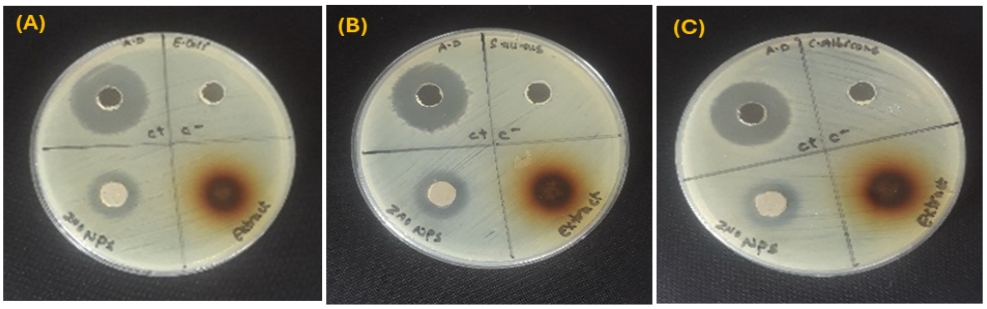


Figure 4. Green ZnO NPs showing antimicrobial activity on microorganisms; (**A**) *Escherichia coli* (**B**) *Staphylococcus aureus*, and (**C**) *Candida albicans*.

Table 3. Inhibition zone (mm) shown by ZnO NPs synthesized from *G. fragrantissima* leaf (Mean ± SD).

Microbes	Reference	Culture Type	Positive Control (C^+) (mm)	ZnO NPs (mm)	Plant Extract (mm)
Escherichia coli	ATCC 8739	Gram −ve	26.0 ± 0.4	17.0 ± 0.2	0
Staphylococcus aureus	ATCC 6538P	Gram +ve	23.0 ± 0.5	17.0 ± 0.3	0
Candida albicans	ATCC 2091	fungi	25.0 ± 0.3	16.0 ± 0.4	0

Porous morphology may enhance surface area and contact with microbial membranes. A more alkaline pH can improve homogeneity and reduce aggregation by better deprotonation of phenolic groups. For ZnO NPs, several factors have been identified for the antimicrobial properties, but the precise mechanism underlying their toxicity remains a subject of ongoing debate. Several unresolved questions within the scope of their antibacterial activity require further investigation. According to earlier research, direct contact with cell membranes, Zn^{2+} ion release, and ROS production are some of the hypothesized mechanisms for antimicrobial activity. These pathways remain hypothetical in the context of our findings because they were not experimentally validated in this work, Figure 5 [46–49]. The medium influences the physicochemical properties of ZnO NPs, altering their mechanisms of toxicity [50]

The production of ROS is considered the main mechanism of ZnO NPs. These ROS, generated from oxygen and water, disrupt the structural integrity of bacterial membranes, leading to cellular damage [51–53]. ZnO has a wide bandgap that behaves like a semiconductor. When light with photon energy greater than the bandgap is absorbed, electrons

in the valence band are excited to the conduction band, creating electron–hole pairs. The absence of electrons in the valence band results in positively charged holes forming [54]. These holes on the ZnO NPs' surface react with water and hydroxyl groups to produce hydroxyl radicals while excited electrons interact with oxygen to form superoxide ions, which can convert into hydroxyl radicals. These highly reactive ROS derivatives damage bacterial cells and inhibit their growth [52,55].

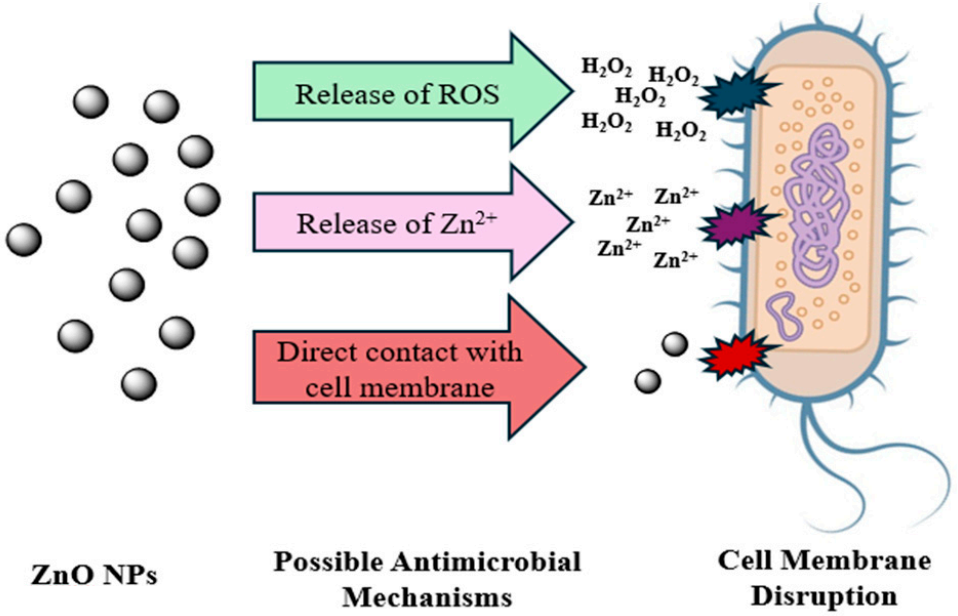


Figure 5. Possible ZnO NPs antimicrobial activity mechanisms include ROS formation, Zn^{2+} release, and direct contact with the cell membrane H_2O_2.

3. Materials and Methods

3.1. Materials

Each of the chemicals employed in this study was of analytical grade and was used without further purification. Zinc nitrate hexahydrate ($Zn(NO_3)_2 \cdot 6H_2O$) with 99.5% purity was sourced from Loba Chemical Pvt. Ltd. in Mumbai, India. Sodium hydroxide (NaOH) with 97% purity was acquired from Thermo Fisher Scientific India Pvt. Ltd. Ethanol with 99.9% purity was obtained from RCP Distilleries India Pvt. Ltd. in Meerut, India. Double distilled water served as the solvent for preparing all solutions. *G. fragrantissima* plants were collected from the local area, Bhotechaur, Melamchi Municipality, ward No. 2, Sindhupalchok district, Nepal, GPS coordinates (latitude: 27.8297° N, longitude: 85.5762° E). The plant was authenticated by the National Herbarium and Plant Laboratory (NHPL), Lalitpur, Nepal.

3.2. Plant Extract Preparation

The harvested plants were collected and dried in a cool, shaded area. The plant features small, leathery, glossy, dark green leaves, as can be seen in Figure 1a. The leaves, after drying in the shade, were pulverized with a mixture grinder (Balttra, STYLO-3 BMG-134, New Delhi, India) and placed in a clean plastic bag for storage. To prepare plant extracts, 5 g of the powdered plant material was combined with distilled water (100 mL), followed by continuous stirring using a magnetic stirrer for about 70 min at approximately 60 °C. The mixture was cooled to room temperature. Finally, the mixture was filtered to remove solid residues, yielding a clear extract. The concentrated extract was collected and appropriately stored for subsequent analyses.

3.3. ZnO NPs Synthesis

ZnO NPs were prepared with minor adjustments to the procedure described by Khadka et al. [34]. A solution was made by dissolving 4 g of $Zn(NO_3)_2 \cdot 6H_2O$ in 100 mL of aqueous plant extract. The pH was adjusted to 10 using 0.1 M NaOH, and the mixture was stirred continuously at 60 °C for two hours. The pH was adjusted to 10 because alkaline conditions favor the deprotonation of phenolic groups in the plant extract, enhancing their reducing ability and promoting efficient nucleation of ZnO NPs [56]. The resulting precipitate was separated through centrifugation, washed thoroughly with ethanol and distilled water, and dried at 80 °C. Calcination at 400 °C for two hours yielded ZnO NPs, which were then stored in an airtight container for further analysis. While only a single synthesis condition (pH 10, 400 °C) was applied here, future work will involve systematic optimization of parameters such as pH and calcination temperature to further enhance NPs characteristics. The crude extract of *G. fragrantissima* was analyzed for secondary metabolites through qualitative phytochemical screening, utilizing the protocols outlined [57,58].

3.4. Characterizations of ZnO NPs

UV–vis spectroscopy was performed using a double-beam spectrophotometer (SPECORD 200 PLUS, Analytik Jena, Jena, Germany) to record the absorbance spectra of ZnO NPs and confirm their formation. The spectra were captured from the 200 nm to 600 nm wavelength range. The dried ZnO NPs were subjected to FTIR analysis using an IRTraacer-100, SHIMADZU, Tokyo, Japan. Spectral data were gathered in the 400–4000 cm^{-1} range. The morphology and elemental composition of the synthesized ZnO NPs were analyzed using a Field Emission Scanning Electron Microscope (FESEM, Hitachi, Tokyo, Japan) integrated with an EDS. Crystal structure and size were examined by XRD. This technique involves directing X-rays at the sample, where they interact with the periodic atomic planes within the crystal lattice, resulting in diffraction. The angles and intensities of these diffracted beams are recorded to produce a unique diffraction pattern of the NP. The crystal structure was studied by XRD (Bruker D2 Phaser, Karlsruhe, Germany) with Cu Kα radiation in the 2θ range of 20°–70°. The Debye–Scherrer equation (Equation (2)) was used to calculate the average crystallite size (D) [59].

$$D = \frac{k.\lambda}{\beta \cos \theta} \quad (2)$$

in which D is the crystallite size (nm), K is the Scherrer constant (0.9), λ is the wavelength of an incident X-ray (1.5406 Å), β is full width at half maximum of peak (FWHM) in radians, and θ is the diffraction angle (radians).

3.5. Antimicrobial Activity

The antimicrobial properties of ZnO NPs and plant extracts were assessed against two bacterial strains—*Escherichia coli* (ATCC 8739), a Gram-negative bacterium, and *Staphylococcus aureus* (ATCC 6538P), a Gram-positive bacterium, as well as one fungal species, *Candida albicans* (ATCC 2091). The evaluation was conducted using the agar well diffusion method to compare their efficacy against a standard antibiotic. Each culture was incubated under optimal conditions, ensuring precise measurement of inhibition zones and clear differentiation between microbial responses.

3.6. Media Preparation

Liquid broth (LB) medium was prepared by dissolving 13 g of LB powder (Sisco Research Laboratories Pvt. Ltd., Mumbai, India) in 1 L distilled water. Then, the solution was autoclaved at 121 °C and 15 psi for 25 min and cooled to 50 °C. Once cooled, the

media was aseptically transferred into sterilized 15 mL Falcon tubes, with 5 mL aliquots per tube. Each tube was then inoculated with a bacterial culture and incubated for 1 day for bacterial cell growth. To ensure accuracy and reproducibility, it is crucial to maintain aseptic techniques throughout the process and to verify that the incubation conditions are optimal for the specific bacterial strains being studied.

3.7. MH Media Plates and Antimicrobial Assay Preparation

Mueller–Hinton Agar (MHA) plates were prepared by dissolving 39 g of MHA powder (Sisco Research Laboratories Pvt. Ltd., Mumbai, India) in 1 L distilled water. Then, sterilizing at 121 °C and 15 psi for 25 min was performed. After autoclaving, the media was cooled to 50 °C and stored in sterile petri dishes, with 25 mL media per dish. Before the antimicrobial assay, each plate (stored in the refrigerator) was labelled with the corresponding sample name. By using a sterile cotton swab, a 150 µL aliquot of bacterial suspension was spread evenly on the surface of the agar. Wells (9 mm diameter, 3 mm depth) were then created in the agar to accommodate the test samples and standards. All samples were loaded at a 50 mg/mL concentration dissolved in dimethyl sulphoxide (DMSO). Each well was filled with 100 µL of the corresponding sample solution. DMSO (C^-) served as the negative control, while kanamycin (5 mg/mL, 10 µL; Sigma-Aldrich, St. Louis, MO, USA, Purity: 95%) was used as the positive control for bacterial strains, and itraconazole (20 mg/mL, 10 µL; Deurali Janta Pharmaceuticals, Kathmandu, Nepal) was used as the positive control for the fungal strain. The plates were stored at 37 °C for 24 h; then, antimicrobial effects were evaluated.

4. Conclusions

This work explores the synthesis, characterization, and antimicrobial properties of ZnO NPs using *G. fragrantissima* leaf extract. FTIR, UV–vis, XRD, and FESEM with EDX spectroscopy techniques are used for the characterization of synthesized NPs. XRD showed the crystalline structure of a nanoparticle size of 8.26 nm, while UV–vis identified characteristic optical absorption peaks. FTIR revealed functional groups from the plant extract. The FESEM-EDX analysis confirmed irregular morphology and a high weight percentage of Zn and oxygen. Phytochemical analysis of the *G. fragrantissima* methanol extract detected alkaloids, flavonoids, tannins, phenols, and other bioactive compounds, though proteins and amino acids were absent. Using the agar well diffusion technique, antimicrobial activity demonstrated moderate inhibition against bacterial and fungal pathogens, with inhibition zones of 16–17 mm. The aqueous plant extract displayed no antimicrobial effect, likely due to poor extraction efficiency. ZnO NPs demonstrated promising antimicrobial potential, while the plant extract's activity could be further explored with improved extraction techniques. Future research will focus on finding the minimum inhibitory concentration (MIC), checking the stability of the plant extract, and improving the synthesis process. This study had some limitations: lack of quantitative phytochemical data and potential variability in extract composition. Although the ZnO NPs showed moderate antimicrobial activity, more studies are needed to fully understand their potential, including MIC/MBC determination and testing against more microbial strains. To gain a better understanding of the mechanistic role of bioactives in the synthesis of NPs, future research should incorporate quantitative estimation of the total phenolic and flavonoid content.

Author Contributions: B.R.P.: Conceptualization, Methodology, Investigation, Validation, Formal analysis, Writing—original draft. S.D. and A.D.: Conceptualization, Writing—review and editing. L.T., A.R.P., and D.K.: Methodology, Data curation, Visualization. M.R.P.: Methodology, Data curation, Visualization, Writing—review and editing. M.B.P., A.A.K. and J.B.: Methodology, Data curation,

Conceptualization, Formal Analysis. All authors have read and agreed to the published version of the manuscript.

Funding: This research received no external funding.

Institutional Review Board Statement: Not applicable.

Informed Consent Statement: Not applicable.

Data Availability Statement: The data presented in this study are available on request from the corresponding authors.

Acknowledgments: Plant identification was performed at the National Herbarium and Plant Laboratories in Godavari, Lalitpur, Nepal.

Conflicts of Interest: The authors declare that they have no known competing financial interests or personal relationships that could have appeared to influence the work reported in this paper.

References

1. Aflakian, F.; Mirzavi, F.; Aiyelabegan, H.T.; Soleimani, A.; Gholizadeh Navashenaq, J.; Karimi-Sani, I.; Rafati Zomorodi, A.; Vakili-Ghartavol, R. Nanoparticles-Based Therapeutics for the Management of Bacterial Infections: A Special Emphasis on FDA Approved Products and Clinical Trials. *Eur. J. Pharm. Sci.* **2023**, *188*, 106515. [CrossRef] [PubMed]
2. Gao, W.; Chen, Y.; Zhang, Y.; Zhang, Q.; Zhang, L. Nanoparticle-Based Local Antimicrobial Drug Delivery. *Adv. Drug Deliv. Rev.* **2018**, *127*, 46–57. [CrossRef] [PubMed]
3. Mercan, D.-A.; Niculescu, A.-G.; Grumezescu, A.M. Nanoparticles for Antimicrobial Agents Delivery—An Up-to-Date Review. *Int. J. Mol. Sci.* **2022**, *23*, 13862. [CrossRef] [PubMed]
4. Balderrama-González, A.-S.; Piñón-Castillo, H.-A.; Ramírez-Valdespino, C.-A.; Landeros-Martínez, L.-L.; Orrantia-Borunda, E.; Esparza-Ponce, H.-E. Antimicrobial Resistance and Inorganic Nanoparticles. *Int. J. Mol. Sci.* **2021**, *22*, 12890. [CrossRef] [PubMed]
5. Spirescu, V.A.; Chircov, C.; Grumezescu, A.M.; Vasile, B.Ș.; Andronescu, E. Inorganic Nanoparticles and Composite Films for Antimicrobial Therapies. *Int. J. Mol. Sci.* **2021**, *22*, 4595. [CrossRef] [PubMed]
6. Tsikourkitoudi, V.; Henriques-Normark, B.; Sotiriou, G.A. Inorganic Nanoparticle Engineering against Bacterial Infections. *Curr. Opin. Chem. Eng.* **2022**, *38*, 100872. [CrossRef]
7. Sirelkhatim, A.; Mahmud, S.; Seeni, A.; Kaus, N.H.M.; Ann, L.C.; Bakhori, S.K.M.; Hasan, H.; Mohamad, D. Review on Zinc Oxide Nanoparticles: Antibacterial Activity and Toxicity Mechanism. *Nano-Micro Lett.* **2015**, *7*, 219–242. [CrossRef] [PubMed]
8. Zhou, X.-Q.; Hayat, Z.; Zhang, D.-D.; Li, M.-Y.; Hu, S.; Wu, Q.; Cao, Y.-F.; Yuan, Y. Zinc Oxide Nanoparticles: Synthesis, Characterization, Modification, and Applications in Food and Agriculture. *Processes* **2023**, *11*, 1193. [CrossRef]
9. Jiang, J.; Pi, J.; Cai, J. The Advancing of Zinc Oxide Nanoparticles for Biomedical Applications. *Bioinorg. Chem. Appl.* **2018**, *2018*, 1062562. [CrossRef] [PubMed]
10. Raha, S.; Ahmaruzzaman, M. ZnO Nanostructured Materials and Their Potential Applications: Progress, Challenges and Perspectives. *Nanoscale Adv.* **2022**, *4*, 1868–1925. [CrossRef] [PubMed]
11. Jung, S.; Lee, J.; Seo, J.; Kim, U.; Choi, Y.; Park, H. Development of Annealing-Free, Solution-Processable Inverted Organic Solar Cells with N-Doped Graphene Electrodes Using Zinc Oxide Nanoparticles. *Nano Lett.* **2018**, *18*, 1337–1343. [CrossRef] [PubMed]
12. Kumar, A. Sol Gel Synthesis of Zinc Oxide Nanoparticles and Their Application as Nano-Composite Electrode Material for Supercapacitor. *J. Mol. Struct.* **2020**, *1220*, 128654. [CrossRef]
13. Özgür, Ü.; Hofstetter, D.; Morkoç, H. ZnO Devices and Applications: A Review of Current Status and Future Prospects. *Proc. IEEE* **2010**, *98*, 1255–1268. [CrossRef]
14. Ayoub, I.; Kumar, V.; Abolhassani, R.; Sehgal, R.; Sharma, V.; Sehgal, R.; Swart, H.C.; Mishra, Y.K. Advances in ZnO: Manipulation of Defects for Enhancing Their Technological Potentials. *Nanotechnol. Rev.* **2022**, *11*, 575–619. [CrossRef]
15. Sagheer, R.; Khadija, S.T.; Kayani, Z.N.; Riaz, S. Structural, optical and magnetic properties of ZnO nanoparticles tailored by 'La^{3+}' ions. *Optik* **2021**, *244*, 166816. [CrossRef]
16. Dimkpa, C.O.; McLean, J.E.; Britt, D.W.; Anderson, A.J. Bioactivity and Biomodification of Ag, ZnO, and CuO Nanoparticles with Relevance to Plant Performance in Agriculture. *Ind. Biotechnol.* **2012**, *8*, 344–357. [CrossRef]
17. Mittal, D.; Kaur, G.; Singh, P.; Yadav, K.; Ali, S.A. Nanoparticle-Based Sustainable Agriculture and Food Science: Recent Advances and Future Outlook. *Front. Nanotechnol.* **2020**, *2*, 579954. [CrossRef]
18. Sekhon, B. Nanotechnology in Agri-Food Production: An Overview. *Nanotechnol. Sci. Appl.* **2014**, *7*, 31–53. [CrossRef] [PubMed]
19. Hanley, C.; Layne, J.; Punnoose, A.; Reddy, K.M.; Coombs, I.; Coombs, A.; Feris, K.; Wingett, D. Preferential Killing of Cancer Cells and Activated Human T Cells Using ZnO Nanoparticles. *Nanotechnology* **2008**, *19*, 295103. [CrossRef] [PubMed]

20. Premanathan, M.; Karthikeyan, K.; Jeyasubramanian, K.; Manivannan, G. Selective Toxicity of ZnO Nanoparticles toward Gram-Positive Bacteria and Cancer Cells by Apoptosis through Lipid Peroxidation. *Nanomed. Nanotechnol. Biol. Med.* **2011**, *7*, 184–192. [CrossRef] [PubMed]
21. Nair, S.; Sasidharan, A.; Divya Rani, V.V.; Menon, D.; Nair, S.; Manzoor, K.; Raina, S. Role of Size Scale of ZnO Nanoparticles and Microparticles on Toxicity toward Bacteria and Osteoblast Cancer Cells. *J. Mater. Sci. Mater. Med.* **2009**, *20*, 235–241. [CrossRef] [PubMed]
22. Kołodziejczak-Radzimska, A.; Jesionowski, T. Zinc Oxide—From Synthesis to Application: A Review. *Materials* **2014**, *7*, 2833–2881. [CrossRef] [PubMed]
23. Talebian, N.; Amininezhad, S.M.; Doudi, M. Controllable Synthesis of ZnO Nanoparticles and Their Morphology-Dependent Antibacterial and Optical Properties. *J. Photochem. Photobiol. B Biol.* **2013**, *120*, 66–73. [CrossRef] [PubMed]
24. Ali, A.; Phull, A.-R.; Zia, M. Elemental Zinc to Zinc Nanoparticles: Is ZnO NPs Crucial for Life? Synthesis, Toxicological, and Environmental Concerns. *Nanotechnol. Rev.* **2018**, *7*, 413–441. [CrossRef]
25. Osman, A.I.; Zhang, Y.; Farghali, M.; Rashwan, A.K.; Eltaweil, A.S.; El-Monaem, E.M.A.; Mohamed, I.M.A.; Badr, M.M.; Ihara, I.; Rooney, D.W. Synthesis of green nanoparticles for energy, biomedical, environmental, agricultural, and food applications: A review. *Environ. Chem. Lett.* **2024**, *22*, 841–887. [CrossRef]
26. Jain, K.; Takuli, A.; Gupta, T.K.; Gupta, D. Rethinking Nanoparticle Synthesis: A Sustainable Approach vs. Traditional Methods. *Chem. Asian J.* **2024**, *19*, e202400701. [CrossRef] [PubMed]
27. Pandey, B.P.; Thapa, R.; Upreti, A. Chemical Composition, Antioxidant and Antibacterial Activities of Essential Oil and Methanol Extract of Artemisia Vulgaris and Gaultheria Fragrantissima Collected from Nepal. *Asian Pac. J. Trop. Med.* **2017**, *10*, 952–959. [CrossRef] [PubMed]
28. Michel, P.; Granica, S.; Magiera, A.; Rosińska, K.; Jurek, M.; Poraj, Ł.; Olszewska, M.A. Salicylate and Procyanidin-Rich Stem Extracts of Gaultheria Procumbens L. Inhibit Pro-Inflammatory Enzymes and Suppress Pro-Inflammatory and Pro-Oxidant Functions of Human Neutrophils Ex Vivo. *Int. J. Mol. Sci.* **2019**, *20*, 1753. [CrossRef] [PubMed]
29. Michel, P.; Dobrowolska, A.; Kicel, A.; Owczarek, A.; Bazylko, A.; Granica, S.; Piwowarski, J.; Olszewska, M. Polyphenolic Profile, Antioxidant and Anti-Inflammatory Activity of Eastern Teaberry (*Gaultheria Procumbens* L.) Leaf Extracts. *Molecules* **2014**, *19*, 20498–20520. [CrossRef] [PubMed]
30. Ahmad, T.; Bustam, M.A.; Irfan, M.; Moniruzzaman, M.; Asghar, H.M.A.; Bhattacharjee, S. Mechanistic Investigation of Phytochemicals Involved in Green Synthesis of Gold Nanoparticles Using Aqueous Elaeis Guineensis Leaves Extract: Role of Phenolic Compounds and Flavonoids. *Biotechnol. Appl. Biochem.* **2019**, *66*, 698–708. [CrossRef] [PubMed]
31. Yagoub, A.E.A.; Al-Shammari, G.M.; Al-Harbi, L.N.; Subash-Babu, P.; Elsayim, R.; Mohammed, M.A.; Yahya, M.A.; Fattiny, S.Z.A. Antimicrobial Properties of Zinc Oxide Nanoparticles Synthesized from Lavandula Pubescens Shoot Methanol Extract. *Appl. Sci.* **2022**, *12*, 11613. [CrossRef]
32. Saranya, K.S.; Vellora Thekkae Padil, V.; Senan, C.; Pilankatta, R.; Saranya, K.; George, B.; Wacławek, S.; Černík, M. Green Synthesis of High Temperature Stable Anatase Titanium Dioxide Nanoparticles Using Gum Kondagogu: Characterization and Solar Driven Photocatalytic Degradation of Organic Dye. *Nanomaterials* **2018**, *8*, 1002. [CrossRef] [PubMed]
33. Abdelbaky, A.S.; Mohamed, A.M.H.A.; Sharaky, M.; Mohamed, N.A.; Diab, Y.M. Green Approach for the Synthesis of ZnO Nanoparticles Using Cymbopogon Citratus Aqueous Leaf Extract: Characterization and Evaluation of Their Biological Activities. *Chem. Biol. Technol. Agric.* **2023**, *10*, 63. [CrossRef]
34. Khadka, D.; Bista, P.; Baral, J.; Gautam, S.K.; Bastakoti, B.P.; Poudel, B.R.; Pokhrel, M.R. Green Synthesis of Zinc Oxide Nanoparticles Using Swertia chirayita for Photocatalytic and Antimicrobial Activity. *J. Inst. Sci. Technol.* **2025**, *30*, 45–56. [CrossRef]
35. Xin-Hua, L.; Jia-Yue, X.; Min, J.; Hui, S.; Xiao-Min, L. Electrical and Optical Properties of Bulk ZnO Single Crystal Grown by Flux Bridgman Method. *Chin. Phys. Lett.* **2006**, *23*, 3356–3358. [CrossRef]
36. Debanath, M.K.; Karmakar, S. Study of Blueshift of Optical Band Gap in Zinc Oxide (ZnO) Nanoparticles Prepared by Low-Temperature Wet Chemical Method. *Mater. Lett.* **2013**, *111*, 116–119. [CrossRef]
37. Baral, J.; Pokharel, N.; Dhungana, S.; Tiwari, L.; Khadka, D.; Pokhrel, M.R.; Poudel, B.R. Green Synthesis of Copper Oxide Nanoparticles Using Mentha (Mint) Leaves Characterization and Its Antimicrobial Properties with Phytochemicals Screening. *J. Nepal Chem. Soc.* **2025**, *45*, 111–121. [CrossRef]
38. Basnet, P.; Samanta, D.; Inakhunbi Chanu, T.; Mukherjee, J.; Chatterjee, S. Assessment of synthesis approaches for tuning the photocatalytic property of ZnO nanoparticles. *SN Appl. Sci.* **2019**, *1*, 633. [CrossRef]
39. Khadka, D.; Gautam, P.; Dahal, R.; Ashie, M.D.; Paudyal, H.; Ghimire, K.N.; Pant, B.; Poudel, B.R.; Bastakoti, B.P.; Pokhrel, M.R. Evaluating the Photocatalytic Activity of Green Synthesized Iron Oxide Nanoparticles. *Catalysts* **2024**, *14*, 751. [CrossRef]
40. Ramesh, M.; Anbuvannan, M.; Viruthagiri, G. Green Synthesis of ZnO Nanoparticles Using Solanum Nigrum Leaf Extract and Their Antibacterial Activity. *Spectrochim. Acta Part A Mol. Biomol. Spectrosc.* **2015**, *136*, 864–870. [CrossRef] [PubMed]

41. Rajkumar, C.; Srivastava, R.K. Annealing temperature mediated enhanced photosensitivity in bicone-like and flower-like structures of ZnO synthesized using Co-precipitation method. *Opt. Mater.* **2020**, *109*, 110367. [CrossRef]
42. Singh, A.; Vishwakarma, H.L. Study of structural, morphological, optical and electroluminescent properties of undoped ZnO nanorods grown by a simple chemical precipitation. *Mater. Sci.* **2015**, *33*, 751–759. [CrossRef]
43. Poudel, B.R.; Tiwari, L.; Magar, C.; Dhungana, S.; Poudel, A.R.; Khadka, D.; Pokhrel, M.R.; Baral, J. Eco-friendly synthesis of zinc oxide nanoparticle using Centella asiatica: Phytochemical analysis, characterization and antimicrobial activity assessment. *Sci. World* **2025**, *18*, 39–46. [CrossRef]
44. Suresh, D.; Nethravathi, P.C.; Udayabhanu; Rajanaika, H.; Nagabhushana, H.; Sharma, S.C. Green Synthesis of Multifunctional Zinc Oxide (ZnO) Nanoparticles Using Cassia Fistula Plant Extract and Their Photodegradative, Antioxidant and Antibacterial Activities. *Mater. Sci. Semicond. Process.* **2015**, *31*, 446–454. [CrossRef]
45. Yogamalar, R.; Srinivasan, R.; Vinu, A.; Ariga, K.; Bose, A.C. X-ray peak broadening analysis in ZnO nanoparticles. *Solid State Commun.* **2009**, *149*, 1919–1923. [CrossRef]
46. Adams, L.K.; Lyon, D.Y.; Alvarez, P.J.J. Comparative Eco-Toxicity of Nanoscale TiO2, SiO2, and ZnO Water Suspensions. *Water Res.* **2006**, *40*, 3527–3532. [CrossRef] [PubMed]
47. Kasemets, K.; Ivask, A.; Dubourguier, H.-C.; Kahru, A. Toxicity of Nanoparticles of ZnO, CuO and TiO2 to Yeast Saccharomyces Cerevisiae. *Toxicol. In Vitro* **2009**, *23*, 1116–1122. [CrossRef] [PubMed]
48. Sawai, J.; Shoji, S.; Igarashi, H.; Hashimoto, A.; Kokugan, T.; Shimizu, M.; Kojima, H. Hydrogen Peroxide as an Antibacterial Factor in Zinc Oxide Powder Slurry. *J. Ferment. Bioeng.* **1998**, *86*, 521–522. [CrossRef]
49. Lipovsky, A.; Nitzan, Y.; Gedanken, A.; Lubart, R. Antifungal Activity of ZnO Nanoparticles—The Role of ROS Mediated Cell Injury. *Nanotechnology* **2011**, *22*, 105101. [CrossRef] [PubMed]
50. Li, M.; Zhu, L.; Lin, D. Toxicity of ZnO Nanoparticles to Escherichia Coli: Mechanism and the Influence of Medium Components. *Environ. Sci. Technol.* **2011**, *45*, 1977–1983. [CrossRef] [PubMed]
51. Yamamoto, O. Influence of Particle Size on the Antibacterial Activity of Zinc Oxide. *Int. J. Inorg. Mater.* **2001**, *3*, 643–646. [CrossRef]
52. Król, A.; Pomastowski, P.; Rafińska, K.; Railean-Plugaru, V.; Buszewski, B. Zinc Oxide Nanoparticles: Synthesis, Antiseptic Activity and Toxicity Mechanism. *Adv. Colloid Interface Sci.* **2017**, *249*, 37–52. [CrossRef] [PubMed]
53. Dhungana, S.; Gauli, A.; Tiwari, L.; Khadka, D.; Gautam, S.K.; Pokhrel, M.R.; Poudel, B.R. Synthesis and Characterization of Copper Oxide Nanoparticles Isolated from Acmella oleracea and Study of Antimicrobial and Phytochemical Properties. *Amrit Res. J.* **2024**, *5*, 18–29. [CrossRef]
54. Janotti, A.; Van De Walle, C.G. Fundamentals of Zinc Oxide as a Semiconductor. *Rep. Prog. Phys.* **2009**, *72*, 126501. [CrossRef]
55. Gordon, T.; Perlstein, B.; Houbara, O.; Felner, I.; Banin, E.; Margel, S. Synthesis and Characterization of Zinc/Iron Oxide Composite Nanoparticles and Their Antibacterial Properties. *Colloids Surf. A Physicochem. Eng. Asp.* **2011**, *374*, 1–8. [CrossRef]
56. Mutukwa, D.; Taziwa, R.; Khotseng, L.E. A Review of the Green Synthesis of ZnO Nanoparticles Utilising Southern African Indigenous Medicinal Plants. *Nanomaterials* **2022**, *12*, 3456. [CrossRef] [PubMed]
57. Aiyegoro, O.A.; Okoh, A.I. Preliminary Phytochemical Screening and In Vitro Antioxidant Activities of the Aqueous Extract of Helichrysum Longifolium DC. *BMC Complement. Altern. Med.* **2010**, *10*, 21. [CrossRef] [PubMed]
58. Harborne, J.B. *Phytochemical Methods*; Springer: Dordrecht, The Netherlands, 1984. [CrossRef]
59. Shrestha, S.; Tiwari, L.; Dhungana, S.; Maharjan, J.; Khadka, D.; Kim, A.A.; Pokhrel, M.R.; Baral, J.; Park, M.; Poudel, B.R. Exploring Photocatalytic, Antimicrobial and Antioxidant Efficacy of Green-Synthesized Zinc Oxide Nanoparticles. *Nanomaterials* **2025**, *15*, 858. [CrossRef] [PubMed]

Disclaimer/Publisher's Note: The statements, opinions and data contained in all publications are solely those of the individual author(s) and contributor(s) and not of MDPI and/or the editor(s). MDPI and/or the editor(s) disclaim responsibility for any injury to people or property resulting from any ideas, methods, instructions or products referred to in the content.